Article

Neuron

Role of Hippocampal CA2 Region in Triggering Sharp-Wave Ripples

Highlights

- Synchronous activity in CA2 region precedes sharp-wave ripples (SPW-Rs).
- Activity of deep CA2 pyramidal cells ramps up before SPW-R, then quickly drops
- Superficial CA2 cells fire synchronously preceding CA3 and CA1 during SPW-Rs
- CA2 cells contribute more strongly to WAKE SPW-Rs while CA3 participates more in SLEEP

Authors

Azahara Oliva,
Antonio Fernández-Ruiz,
György Buzsáki, Antal Berényi

Correspondence

gyorgy.buzsaki@nyumc.org (G.B.),
drberenyi@gmail.com (A.B.)

In Brief

Oliva et al. show that sharp-wave ripple (SPW-R) related activation of CA2 neurons precede those in CA3 and CA1. Deep CA2 cells gradually increase their activity prior to SPW-Rs, establishing the CA2 region as a potential trigger for SPW-R generation.

Oliva et al., 2016, Neuron *91*, 1342–1355
September 21, 2016
http://dx.doi.org/10.1016/j.neuron.2016.08.008

CellPress

CellPress

Neuron
Article

Role of Hippocampal CA2 Region in Triggering Sharp-Wave Ripples

Azahara Oliva,[1] Antonio Fernández-Ruiz,[1,2] György Buzsáki,[3,*] and Antal Berényi[1,3,4,*]
[1]MTA-SZTE "Momentum" Oscillatory Neuronal Networks Research Group, Department of Physiology, University of Szeged, Szeged 6720, Hungary
[2]School of Physics, Complutense University, 28040 Madrid, Spain
[3]New York University Neuroscience Institute and Center for Neural Science, New York University, New York, NY 10016, USA
[4]Lead Contact
*Correspondence: gyorgy.buzsaki@nyumc.org (G.B.), drberenyi@gmail.com (A.B.)
http://dx.doi.org/10.1016/j.neuron.2016.08.008

SUMMARY

Sharp-wave ripples (SPW-Rs) in the hippocampus are implied in memory consolidation, as shown by observational and interventional experiments. However, the mechanism of their generation remains unclear. Using two-dimensional silicon probe arrays, we investigated the propagation of SPW-Rs across the hippocampal CA1, CA2, and CA3 subregions. Synchronous activation of CA2 ensembles preceded SPW-R-related population activity in CA3 and CA1 regions. Deep CA2 neurons gradually increased their activity prior to ripples and were suppressed during the population bursts of CA3-CA1 neurons (ramping cells). Activity of superficial CA2 cells preceded the activity surge in CA3-CA1 (phasic cells). The trigger role of the CA2 region in SPW-R was more pronounced during waking than sleeping. These results point to the CA2 region as an initiation zone for SPW-Rs.

INTRODUCTION

The functioning of the hippocampus is believed to depend on the unique contributions of its subregions and their interactions (Amaral and Lavenex, 2006). Hippocampus proper is made up by divisions of the *cornu Ammonis*, CA1, CA2, and CA3, each with specialized cell types and connectivity (Lorente de Nó, 1947). The vulnerability or resistance of the CA2 region stands out in several pathological conditions, including Alzheimer's disease (Braak et al., 1980), ischemia (Kirino, 1982; Sadowski et al., 1999), hippocampal sclerosis (Babb et al., 1984; Dam, 1980; Gloor, 1991; Kotloski et al., 2002; Sloviter, 1989) and schizophrenia (Benes et al., 1998; Knable et al., 2004; Narr et al., 2004; Nullmeier et al., 2011; Piskorowski et al., 2016; Zhang and Reynolds, 2002). CA3 but not CA2 neurons rapidly degenerate in kainic acid-induced status epilepticus (Nadler et al., 1978). The CA2 region can be clearly delineated from its neighboring regions by expression patterns of several peptides and genes (Kohara et al., 2014; Lein et al., 2004; Young et al., 2006).

Despite these distinct pathophysiological differences, the CA2 region has been traditionally considered as a transition zone, since its pyramidal neurons resemble CA3 neurons both in size and dendritic branching patterns (Ishizuka et al., 1995; Woodhams et al., 1993) and receive inputs from CA3 neurons, similarly to CA1 pyramidal cells (Lorente de Nó, 1947). They also receive input from dentate gyrus granule cells, but they lack the thorny excrescences characteristic of the CA3 neurons (Kohara et al., 2014). In addition to local inputs, CA2 interneurons receive excitation from CA1, CA3, the supramamillary body, and the amygdala (Bartesaghi et al., 2006; Benes and Berretta, 2001; Chevaleyre and Siegelbaum, 2010; Cui et al., 2013; Ding et al., 2010; Kohara et al., 2014; Maglóczky et al., 1994; Mercer et al., 2012; Piskorowski and Chevaleyre, 2012, 2013) and form a loop with layer II entorhinal neurons (Chevaleyre and Siegelbaum, 2010; Rowland and Moser, 2013). In addition to these anatomical differences, recent studies have pointed out the special cognitive and behavioral functions of the CA2 region (Dudek et al., 2016), including its postulated role in social recognition (Alexander et al., 2016; Hitti and Siegelbaum, 2014; Piskorowski et al., 2016; Smith et al., 2016), contextual memory (Alexander et al., 2016; Wintzer et al., 2014), and temporal coding (Mankin et al., 2015).

The hippocampus plays a prominent role in memory consolidation, and hippocampal sharp-wave ripples (SPW-Rs) represent a mechanism of memory transfer from the hippocampus to the neocortex (Buzsáki, 2015; Ego-Stengel and Wilson, 2010; Girardeau et al., 2009; Jadhav et al., 2012). SPW-R complex consists of two components: the sharp wave (SPW) and the ripple. The LFP sharp wave is a negative deflection that reflects the depolarization of the apical dendrites of CA1 pyramidal cells brought about by the synchronous discharge of the CA3 axonal input to those dendrites (Buzsáki et al., 1983; Fernández-Ruiz et al., 2012; Sullivan et al., 2011). On the other hand, the ripple is a ~140 Hz oscillatory event confined to the pyramidal cell body layer and represents a network response of CA1 pyramidal cells and interneurons to the strong synchronous drive (Buzsáki et al., 1992; English et al., 2014; Stark et al., 2014). While the CA3 region is implicated in the generation of the SPW, it is not homogenous in terms of its output pathways and the induction of SPW population bursts (Csicsvari et al., 2000; Mann and Paulsen, 2007). Specifically, whereas pyramidal cells in the CA3a (adjacent to CA2) and distal CA3b subregions give rise to extensive recurrent collaterals that are confined largely to the CA3 region and contribute to the creation of population events, more

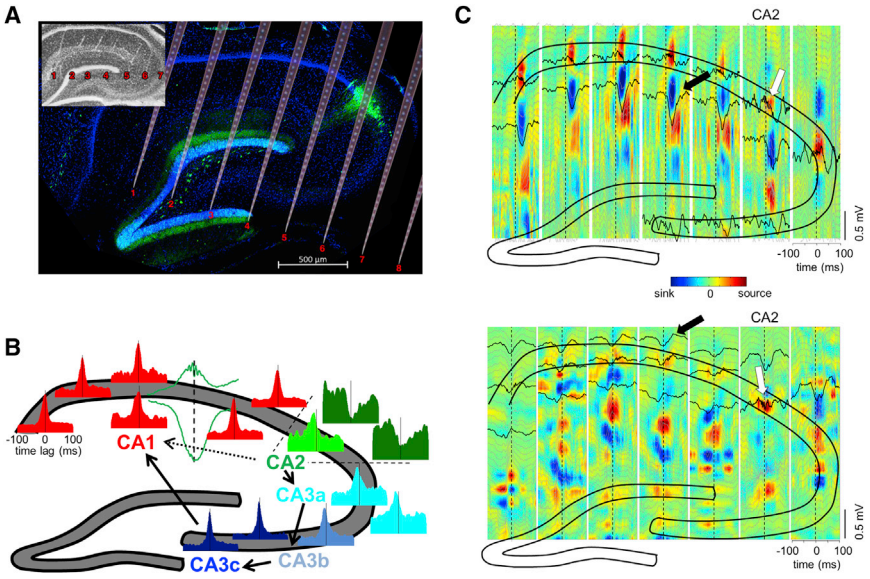

Figure 1. Overview: Heterogeneity of Ripples in CA1, CA2, and CA3 Regions

(A) Histological section parallel to the transverse axis of the hippocampus double stained with DAPI (blue) and anti-PCP4 (green) to identify the CA2 region. The cartoon of the electrode shanks is constructed following the track marks visible on the inset.

(B) Example peri-SPW-R firing histograms of CA1-CA2-CA3a, b, and c pyramidal cells, triggered by the SPW troughs. Histograms are color coded to mark their regions of origin. All histograms are remarkably similar with the exception of a subpopulation of CA2 cells. CA2 boundaries are marked with dashed lines. An example CA1 SPW-R used as trigger is shown in green. Arrows illustrate the expected propagation of synchronous unit firing during SPW-Rs based on the anatomy. From CA2, excitation propagates to CA3a, b, and c and then to CA1. Alternatively, CA2 activity can also propagate directly to CA1 (dashed line).

(C) Upper panel: LFP-CSD map triggered by one CA2 ripple (white arrow). Note the characteristic negative SPW (black lines) and sinks in the str. radiatum (in blue, marked by arrow) accompanied by ripples (black lines) and flanked by passive sources in the pyramidal layer and str. lacunosum-moleculare (red) after the CA2 ripple peak. Bottom panel: Another characteristic pattern triggered by CA2 ripple (white). Excitatory currents in CA1 in str. oriens (blue sinks and black negative waves, black arrow) were accompanied by return currents in str. radiatum (red sources). Note ripples in all CA1 pyramidal layer sites. See also Figure S1.

proximal CA3b and CA3c (adjacent to dentate hilus) neurons send the majority of their axon collaterals to the CA1 region and convey CA3-generated activity to CA1 (Ishizuka et al., 1990; Li et al., 1994). Because the CA2 region mirrors several aspects of CA3 (Tamamaki et al., 1988), its role in SPW-R generation should also be considered. We show here that CA2 neurons are the first neurons to ramp up their activity prior to SPW-Rs and thus play a leading role in their initiation.

RESULTS

We recorded both LFP and unit firing from all layers of the CA1-CA2-CA3 regions in the dorsal hippocampus in behaving rats. Eight animals were implanted with high-density silicon probes (256 recording sites on eight shanks, 32 recording sites on each shank, with 50 μm vertical site separation) parallel to the transverse axis of the dorsal hippocampus. After the recordings, the electrode tracks were determined by histological reconstruction (Figure 1A; Table S1). The CA1-CA2 border was identified by the widening of the pyramidal layer and the larger size of the neurons in the CA2 region and further validated by immunolabeling by the CA2-specific marker PCP4 (Kohara et al., 2014; Valero et al., 2015). The CA3 region was divided into three subregions (Figure 1B): CA3a (closest to CA2), CA3b, and CA3c (see Supplemental Experimental Procedures). All analyses were performed during non-REM sleep (SLEEP) and waking immobility (WAKE).

Brain State-Dependent SPW-Rs in CA1, CA2, and CA3 Areas

LFP ripples reflect organized population spike series of local neurons, temporally coordinated within and across regions by the slower SPW (Schlingloff et al., 2014; Stark et al., 2014; Sullivan et al., 2011; Ylinen et al., 1995). SPW-R events showed varying LFP patterns and current sinks and sources depending on the location of the reference ripple events. Fast oscillatory patterns (100–250 Hz) in the CA1 and CA3 pyramidal layer were characteristically accompanied by a negative SPW (and a sink in the CSD map) in the hippocampal stratum radiatum of CA1-CA3 (Figure S1). This sink in stratum radiatum was flanked by two sources (Figure S1) in strata pyramidale and lacunosum-moleculare (Fernández-Ruiz et al., 2012; Sullivan et al., 2011). In contrast, ripples detected in CA2 had two different LFP patterns. The first type (Figure 1C upper panel) preceded the CA1 SPW and ripple by 10–20 ms. The second type of CA2 ripple (Figure 1C lower panel) was followed by a short latency (~5 ms) negative wave (sink in the CSD map) in CA1 stratum oriens and a corresponding source in stratum radiatum. Depending on the magnitude of the CA1 stratum oriens sink, ripples in the CA1 pyramidal layer could either be present (Figure 1C bottom panel) or not.

To characterize localized activity at the time of the CA1 sharp wave, we computed wavelet spectrograms from 200 ms-long LFP segments recorded from the middle of the pyramidal layer at every recording location in the CA1-2-3 axis, centered at the trough of the large negative SPW in the CA1 stratum radiatum. As expected, strong ripple-band power (at ~150 Hz) appeared at all CA1 sites during SPW events during both SLEEP and WAKE states. SPWs and ripples were generally coherent in the transverse axis (Figure S1; Patel et al., 2012). In contrast, CA2 and CA3 activity was divergent and depended on brain state (Figure 2A). First, the peak of ripple power in CA2 significantly preceded the CA1 SPW trough during both SLEEP and WAKE (white asterisks, Figure 2B; $p < 0.001$; t test; $n = 16$ sessions in five rats), whereas CA3 peak power trailed behind ($p < 0.001$, t test; $n = 20$ sessions in seven rats). Second, during SLEEP

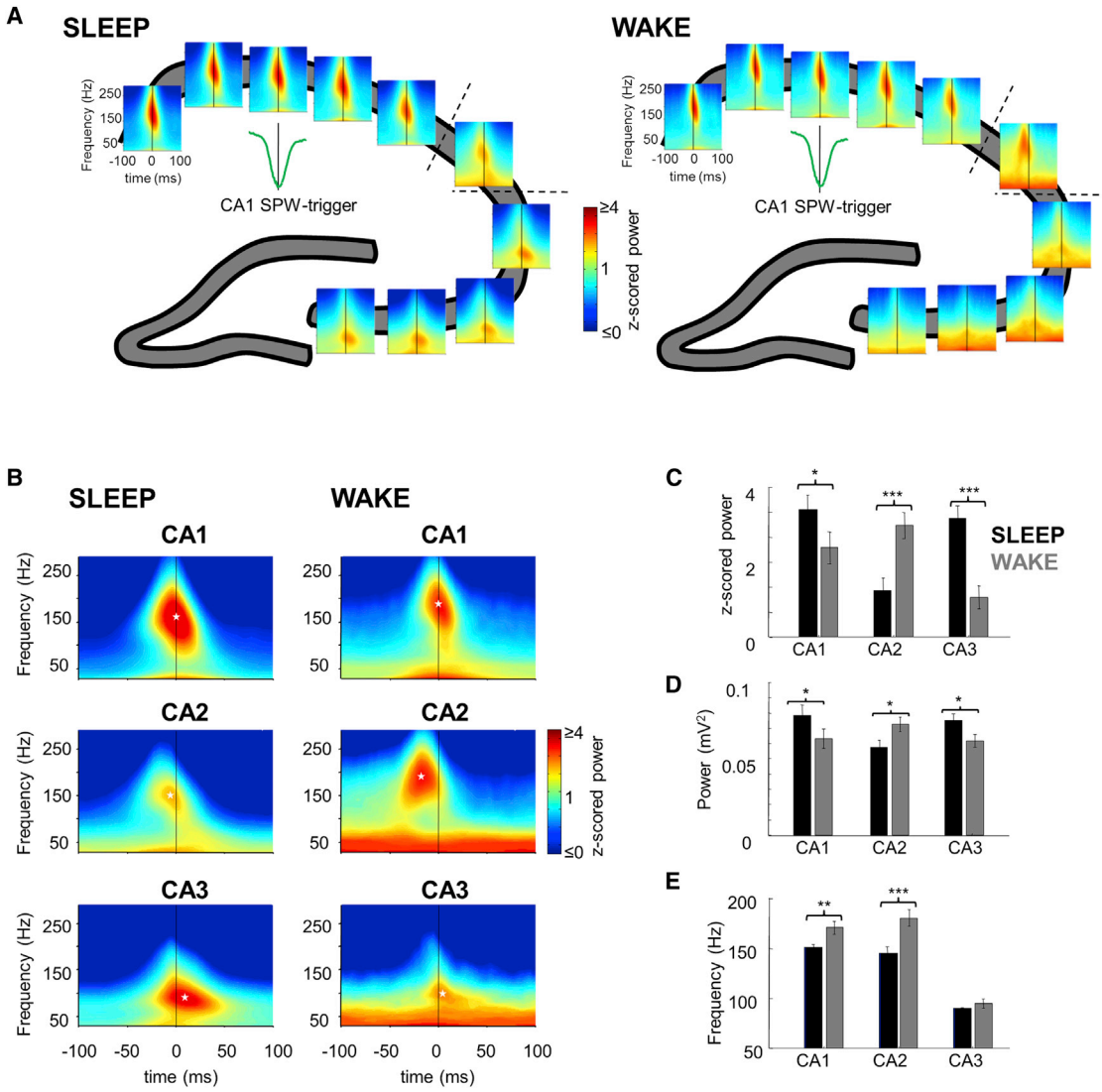

Figure 2. High-Frequency LFP Oscillations during SPW-R

(A) An example of SPW-R triggered wavelet spectrograms at every recording site in the CA1-CA2-CA3 pyramidal layer during a single session. Strong power increase in the ripple band appeared at every site during both SLEEP and WAKE SPW-R, albeit with different timing and frequency profiles.

(B) Averaged SPW-R-triggered spectrograms of the different regions for both states. Ripple power in CA1 appeared synchronously with SPW-R peak; however, it appeared earlier in CA2, while later and with slower frequency in CA3. Black lines, SPW trough; white asterisks, maximal ripple powers.

(C) Ripple power was significantly larger in CA2 during WAKE ripples, while in CA1 and CA3 during SLEEP ripples.

(D) Same comparisons as (C) but with absolute voltage values showing similar results.

(E) Frequency of power maximum is similar in CA1 and CA2 regions and higher during WAKE, and ripple frequency is significantly slower in CA3.

See also Figure S2. Error bars in (C), (D), and (E) represent ±SEM.

ripple power in both CA1 and CA3 region was stronger than during WAKE, whereas in CA2 it was stronger during WAKE compared to SLEEP (Figure 2C, *Z* scored power; $p_{CA1} < 0.05$, n = 24 sessions in eight rats; $p_{CA2} < 0.001$, n = 16 sessions in five rats; $p_{CA3} < 0.001$, n = 20 sessions in seven rats; paired t test. Figure 2D, absolute power; $p < 0.05$ all comparisons, paired t test). Third, LFP frequency was comparable in CA1 and CA2 and significantly higher during WAKE than SLEEP (Figure 2D; $p_{CA1} < 0.01$; $p_{CA2} < 0.001$; paired t test). In contrast, in CA3 ripple frequency during CA1, SPW was comparable during SLEEP and WAKE and significantly lower than ripple frequency in either CA1 or CA2 ($p < 0.001$, unpaired t test; all comparisons). Similar results were obtained when CA2 or CA3 ripples were used as the temporal reference (Figure S1).

The above analysis sampled the different subregions only in the time windows of the CA1 SPW-Rs. As a complementary approach, we detected putative ripples independently in the CA1, CA2, and CA3 pyramidal layers (Figure S2). The LFP ripple detection algorithm, tuned to CA1 ripples, detected numerous high-frequency events in the pyramidal layer of CA1, CA2, and

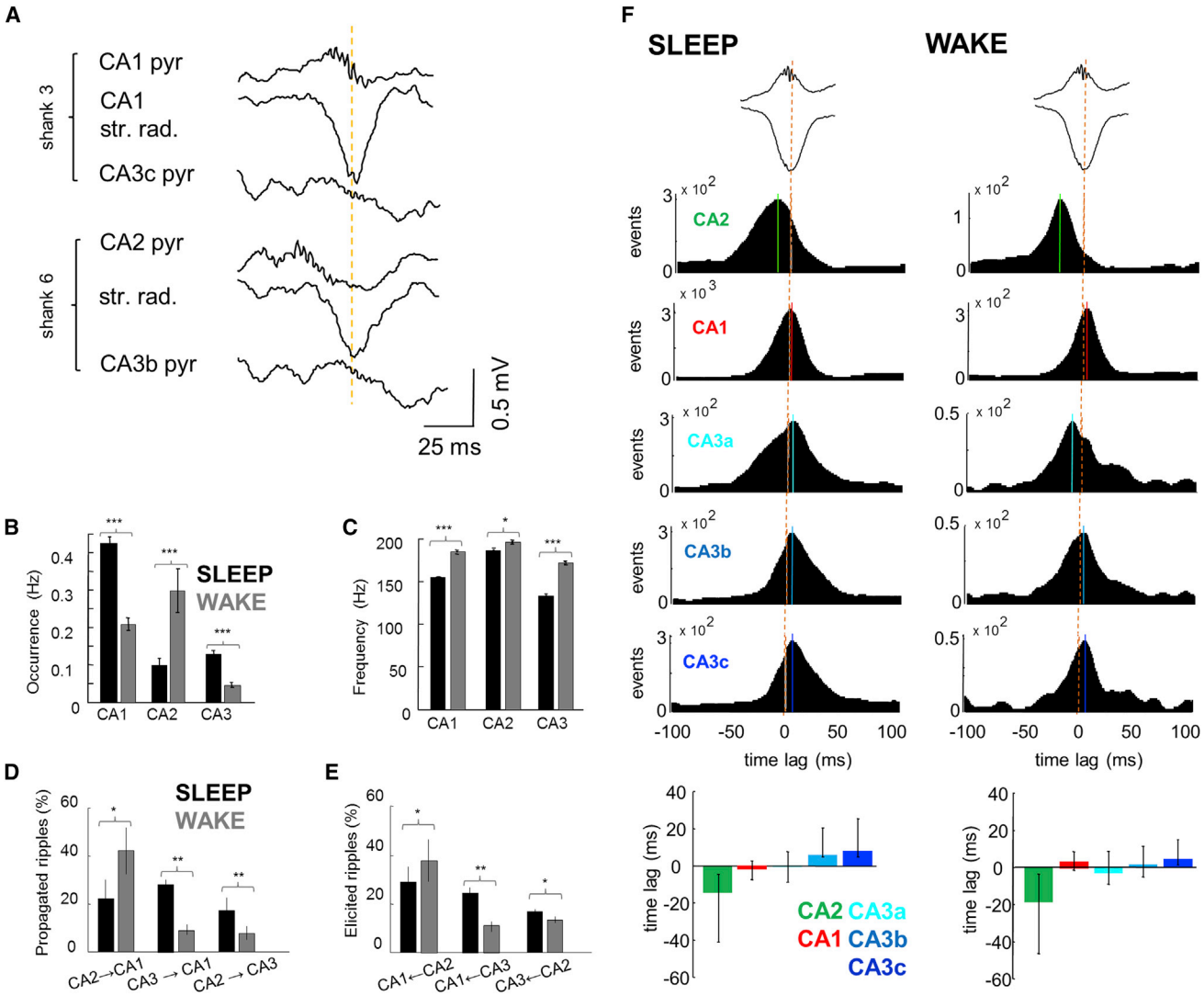

Figure 3. Temporal Relation of Ripples in CA1, CA2, and CA3

(A) Example SPW-R recorded by two shanks, one in CA2 and the other in mid-CA1 region (900 μm distance), both reaching also the CA3 pyramidal layer. Note that while SPWs in CA2 and CA1 are largely synchronous (yellow line), ripple in CA2 occurs 20 ms prior to CA1.

(B) Average occurrence of ripples is higher in CA1 and CA3 during SLEEP compared to CA2, whereas during WAKE CA2 is more active.

(C) Mean frequency (±SEM) of ripples is higher in all regions during WAKE.

(D) Percentages (±SEM) of ripples detected in different regions propagating to downstream areas. Higher proportion of events propagated during WAKE than SLEEP from CA2 to CA1, while from CA3 to CA1 the propagation is larger during SLEEP than WAKE.

(E) The percentage of CA1 ripples that have a previous CA2 ripple is higher during WAKE, and those with a preceding CA3 ripple are more during SLEEP.

(F) Cross-correlograms between ripple peaks and SPW through (orange dashed lines) were constructed by detecting ripples independently at each recording site and pooling data for all sites and animals from the same area. While the peak of ripple power and SPW troughs are aligned in CA1, CA2 ripples occur earlier (13 and 21 ms in SLEEP and WAKE). Solid lines indicate CCG peaks. Median and second/third quartiles of the cross-correlogram distribution emphasize the earlier occurrence of CA2 ripples. See also Figure S2.

CA3 regions (Figure 3A). CA1 and CA3 events were more frequent during SLEEP (Figure 3B; $p < 0.001$ in both regions; n = 116,115/11,595 CA1 events in SLEEP/WAKE in eight rats and n = 13,486/1,273 CA3 events in seven rats; paired t test), whereas in CA2 their occurrence was higher during quiet WAKE (Figure 3B; $p < 0.001$; n = 10,580/3,770 events in five rats; paired t test). The oscillation frequency was faster during WAKE compared to SLEEP in each region (Figure 3C; $p < 0.001$ CA1 and CA3; $p < 0.05$ CA2 for all pooled events; paired t test), and CA2 ripples were significantly faster than ripples in CA1 (SLEEP, $p < 0.001$; WAKE, $p < 0.05$, unpaired t test) or CA3 (SLEEP $p < 0.001$; WAKE, $p < 0.01$; unpaired t test).

Next, we calculated the proportion of ripples detected in CA3 and CA2 that propagated to the CA1 or CA3 regions, respectively (Supplemental Experimental Procedures). A large proportion of CA2 ripples propagated to CA1 and to a lesser extent to

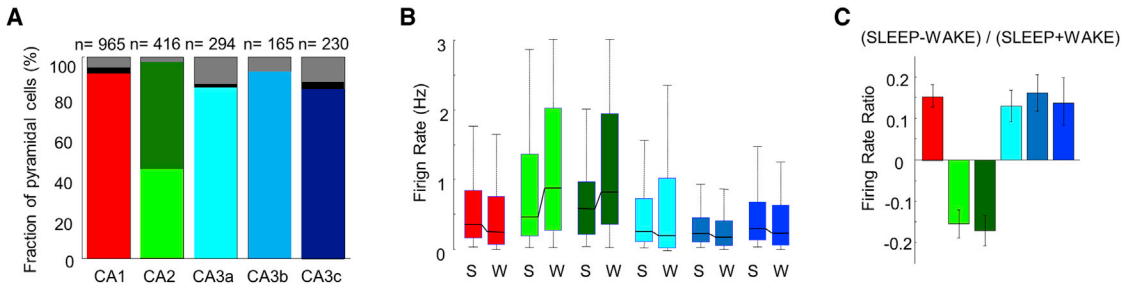

Figure 4. Characteristics of Pyramidal Cells in CA1, CA2, and CA3 Regions

(A) Percentage of cells per region that significantly increased or reduced their firing rates during CA1 SPW-R. Bottom part of each bar represents positively modulated percent of cells, middle part (black or dark green) represents negatively modulated cells, and gray represents non-modulated cells. Note that while only a minority of cells is suppressed in most regions (black), approximately half of the CA2 pyramidal cells reduce their firing rates during SPW-Rs (dark green).

(B) Median firing rates (boxes, interquartile ranges; error bars, ranges) of CA1, CA2, and CA3 pyramidal cells during SLEEP and WAKE. CA2 pyramidal cells fired faster in both states compared to CA1 and CA3 ($p < 0.01/0.001$ for all comparisons during SLEEP and WAKE, Wilcoxon rank-sum test).

(C) While CA1 and CA3 pyramidal cells fired more during SLEEP than WAKE, CA2 principal cells showed the opposite behavior.

Error bars represent ±SEM. See also Figure S3.

CA3 (Figure 3D). During SLEEP, a similar fraction of CA2 ripples propagated to CA1 and CA3 (22%/18%, $p > 0.05$, paired t test), but during WAKE this fraction increased in CA1 (43%, $p < 0.05$, paired t test) and decreased in CA3 (9%, $p < 0.01$, paired t test). In a complementary analysis, we assessed the proportion of CA1- and CA3-detected ripples that were preceded by CA2 or CA3 ripple. This analysis provided similar results (Figure 3E).

To examine the direction of propagation during SPW-Rs, we calculated temporal cross-correlograms between peak times of ripple power in each hippocampal region and the reference SPW trough in CA1 stratum radiatum (Figure 3F). In both SLEEP and WAKE, the peak power of the fast oscillation in both CA1 and CA3 regions were largely aligned with the CA1 SPW troughs (Figure 3F). In contrast, the CA2 region lead the CA1 SPW trough during SLEEP and even more so during WAKE (Figure 3F; $p < 0.001$; paired t test). Comparison of the median time lags of all SPW-ripple power cross-correlograms further illustrates the leading role of CA2 and cascade of events to CA1 and CA3a, b, and c (Figure 3F bottom panels). Congruent results were obtained when different temporal references were used (e.g., SPW onset or CA2 ripple peak; Figure S2). In summary, the LFP analysis suggests that SPW-Rs are often initiated in the CA2 region during SLEEP and even more frequently during WAKE.

Firing Patterns of CA1, CA2, and CA3 Neurons

To examine the neuronal spike correlates of SPW-Rs, neurons were clustered and separated into putative pyramidal cells and interneurons (Supplemental Experimental Procedures). Only pyramidal neurons were included in the analysis unless otherwise noted. First, we classified all neurons according to whether they were significantly modulated by SPW-R or not (Figures 1B and 4A; Figure S3). Most pyramidal neurons in CA1 and CA3 had a significant positive modulation by SPW-Rs (95%/87%/93%/90% in CA1, CA3a, CA3b, and CA3c, respectively; Figure 4A), whereas a minority of pyramidal cells decreased their rates during SPW-Rs (2%/1%/0%/2.5% in CA1, CA3a, CA3b, and CA3c, respectively). In contrast, in CA2, less than half of neurons were positively modulated by SPW-Rs (45%), and a greater proportion (54%) were suppressed (Figure 4A). Thus, we termed these two neuron types as "phasic" (positively modulated) and "ramping" (negatively modulated) cells (Figures 1B and 4A; Figure S3). The majority of putative interneurons (>88%) in CA1, CA2, and CA3 region significantly increased their firing rates during SPW-Rs (Figure S5C). Examples of peri-SPW-ripple firing patterns in different hippocampal regions are illustrated in Figure 1B and Figure S3.

The median firing rates of CA2 pyramidal cells were higher in SLEEP and WAKE than those in CA1 and CA3a, CA3b, and CA3c subregions (Figure 4B; $p < 0.01/0.001$ for SLEEP and WAKE, respectively of all comparisons; n = 965 putative CA1 pyramidal neurons in eight rats; n = 230 putative CA3c pyramidal neurons in six rats, n = 165 putative CA3b pyramidal neurons in seven rats, n = 294 putative CA3a pyramidal neurons in five rats; n = 188 and 228 putative CA2 phasic and CA2 ramping cells in five rats; see below; Wilcoxon rank-sum test). State-dependent modulation of CA2 pyramidal cells was different from CA1 and CA3; they increased their firing rates during WAKE compared to SLEEP, whereas CA1 and CA3 neurons had lower firing rates during WAKE (Figure 4C; $p < 0.001$ for all regions, Wilcoxon signed-rank test). These results indicate that the baseline firing rates of CA2 neurons are higher than those of CA1 or CA3 pyramidal cells, and this difference is magnified during WAKE, similar to a recent report (Kay et al., 2016).

CA2 Ensemble Activity Precedes SPW-Rs

CA1 and CA3a, b, and c neurons fire robustly during SPW-Rs (Csicsvari et al., 2000; Sullivan et al., 2011), and we confirmed this pattern (Figure 5A; n = 965 putative CA1 pyramidal cells in eight rats; n = 230 (six rats), 165 (seven rats), 294 (five rats) pyramidal cells in CA3c, CA3b, and CA3a, respectively; n = 188 CA2 phasic and n = 228 ramping cells in five rats; Wilcoxon rank-sum test). In agreement with the anatomical connectivity of the CA3 recurrent circuit, the earliest-firing neurons in the CA3 region during SLEEP SPW-Rs were the CA3a cells with the strongest recurrent connections (Li et al., 1994), followed by CA3b and c cells (Csicsvari et al., 2000; Figure 5A; $p < 0.001$ for all comparisons, t test). The synchronous discharge of the CA3c neurons and their

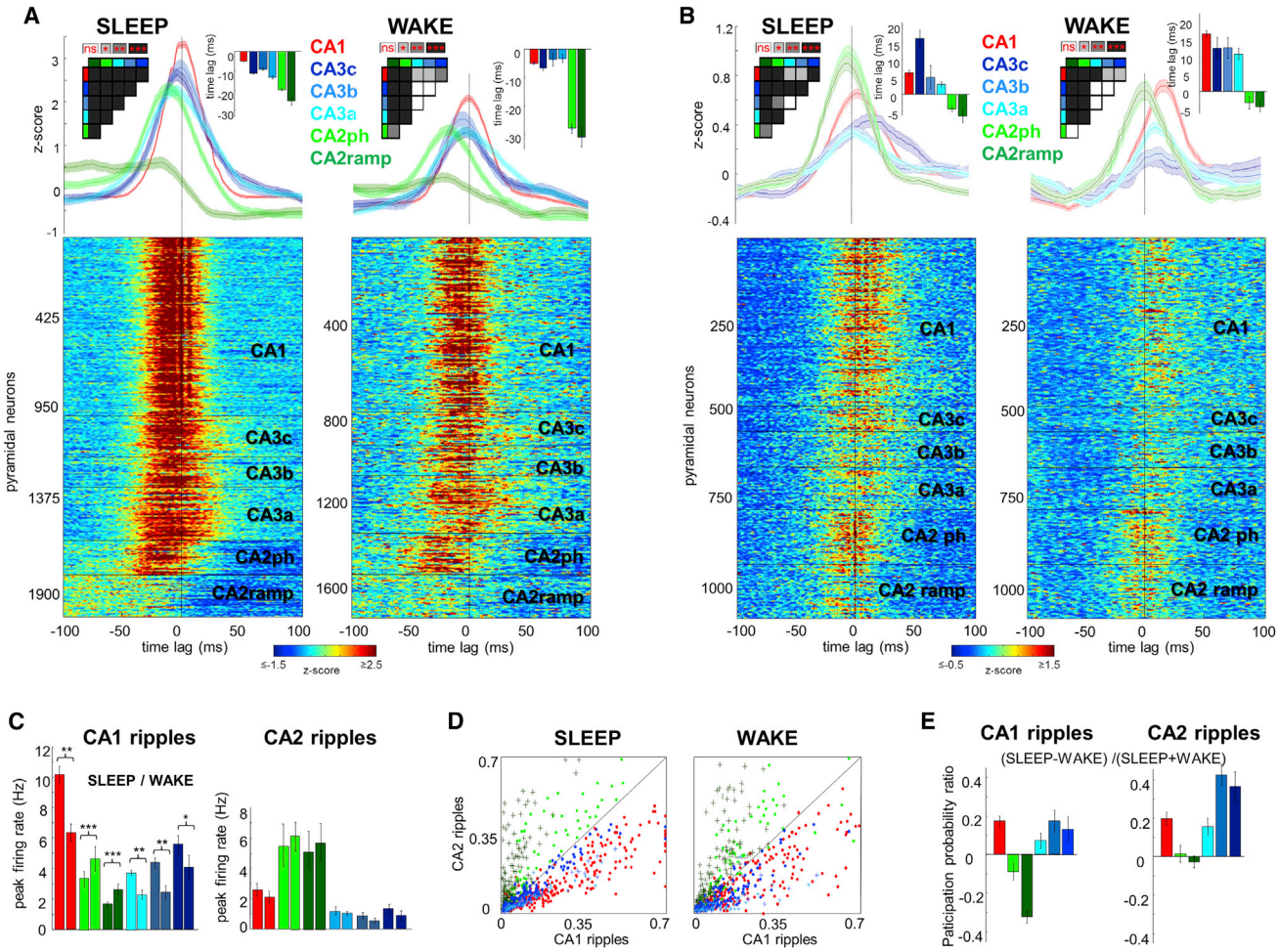

Figure 5. Temporal Dynamics of Unit Activity during CA1 and CA2 Ripples

(A) Peri-SPW-R *Z* scored firing rate raster plots for all putative principal cells and average (±SEM) firing rate curves per region show a propagation of peri-SPW-R activity from CA2 to CA3a, b, and c and finally CA1 during SLEEP (left panel). CA2 cells are separated into two subgroups based on their firing pattern during SPW-R ("phasic" cells, light green; "ramping" cells, dark green). Note the slow early ramping-up and sudden decrease of the firing rate in the ramping group approximately 30 ms prior to CA1 ripple peak. Insets show peak time-lags of averaged firing rate curves, and their color-coded pairwise significance levels. During WAKE SPW-Rs (right), both CA2 cell groups had the highest firing probability 20–30 ms before the SPW-R peak.

(B) Peri-CA2-ripple firing plots were constructed in the same manner as in (A).

(C) Averaged peri-SPW-R firing rate curves (±SEM) in absolute units (Hz) in a ± 100 ms window centered on CA1 ripple peak (left panel). CA1 and CA3 pyramidal cells fired more during SLEEP compared to WAKE. In contrast, CA2 cells fired more during WAKE than SLEEP CA1 ripples. During CA2 ripples (right panel), the firing of CA1 and CA3 units was lower compared to CA1 ripples ($p < 0.001$ for all comparisons, t test) while CA2 pyramidal cells were more active ($p < 0.001$ in both cases). Firing rates were decreased during WAKE in all regions.

(D) Participation probability of CA1, CA2, and CA3 pyramidal cells in CA1 and CA2 ripples illustrates the relative independence of the CA2 region. CA1 and CA3 units have larger degree of participation in CA1 ripples in both states ($p < 0.001$ for all comparisons, signed-rank test), while CA2 units show the opposite behavior ($p < 0.001$ for all comparisons). Note that CA2 phasic cells (light green) have larger degree of participation in both types of ripples than CA2 ramping cells (dark green).

(E) Participation probability of CA1 and CA3 pyramidal cells was higher in CA1 and CA2 ripples during SLEEP compared to WAKE ($p < 0.001$ for CA1 and $p < 0.01$ for CA3a, b, and c in both types of ripples, signed-rank test). In contrast, CA2 units participated more frequently in CA1 ripples during WAKE ($p < 0.01/0.001$ for CA2 phasic/ramping, signed-rank test) but no brain state dependence was present for CA2 ripples ($p > 0.05$).

Error bars represent ±SEM. See also Figures S4, S5, and S6.

excitatory effect then brought about a strong depolarization in the CA1 stratum radiatum, manifested in the LFP as the SPW (Csicsvari et al., 2000; Fernández-Ruiz et al., 2012; Sullivan et al., 2011). SPW-R-related firing of CA2 phasic neurons fitted this general picture, except that they fired earlier ("phasic" CA2 cells; mean time lead of peak firing 18 ± 0.5/28 ± 0.9 ms prior to CA1 SPW-R peak in SLEEP and WAKE; $p < 0.001$ for all comparisons with CA1 and CA3 cells, t test). In contrast, neurons in the ramping subgroup gradually elevated their firing prior to the CA1 SPW-R peak (25 ± 2.5/33 ± 2.3 ms prior to CA1 SPW trough in SLEEP and WAKE, respectively; $p < 0.001$ for all comparisons with CA1 and CA3 cells, t test), fired less

synchronously, and became strongly suppressed subsequently during SPW-Rs (Figure 5A).

Neurons in CA1 and CA3 subregions fired less during WAKE SPW-Rs compared to SLEEP (Figure 5C; CA1: WAKE 6.8 ± 0.7 Hz versus SLEEP 10.2 ± 0.7 Hz, $p < 0.01$, paired t test; CA3: WAKE, 2.4 ± 0.3 Hz/2.5 ± 0.4 Hz/4.4 ± 0.9 Hz versus SLEEP, 4.1 ± 0.4 Hz/4.8 ± 0.4 Hz/5.6 ± 0.3 Hz for CA3a, b, and c, respectively; $p < 0.01/0.01/0.05$; paired t test). In contrast, both subpopulations of CA2 neurons were more active during WAKE SPW-Rs (WAKE, 4.4 ± 0.8 Hz/3.0 ± 0.3 Hz versus SLEEP, 3.0 ± 0.5 Hz/2.0 ± 0.2 Hz for CA2 phasic and ramping groups, respectively; both $p < 0.001$, paired t test), suggesting a stronger CA2 control of SPW-Rs in the waking animal.

When LFP ripples in the CA2 region were chosen as a reference event, both phasic and ramping CA2 pyramidal neurons were strongly recruited to the population event (Figures 5B and 5C; SLEEP phasic cells: 5.7 ± 1.2 Hz peak firing rate; ramping cells: 4.8 ± 1.0 Hz; $p < 0.05$; WAKE phasic cells: 6.4 ± 0.8 Hz peak firing rate; ramping cells: 5.7 ± 1.0 Hz). Notably, CA2 ramping cells did not show the same slow ramping behavior as with CA1-detected ripples (Figure 5B). CA2 ripples may often remain localized, in which case ripples recruited both ramping and phasic neurons in different proportions, leading to a temporal blurring of the two groups (Figure S4F). CA2 spikes associated with local CA2 ripples induced a negative SPW in stratum oriens (sink) and a positive return current in stratum radiatum, whereas CA2 spikes that were associated with CA3-CA1 propagating ripples induced negative SPWs in stratum radiatum (Figure S4E). While CA2 pyramidal neurons fired maximally 2–5 ms before the peak power of local ripples, CA3 and CA1 pyramidal cells fired after the peak of CA2 ripples. Similar results were obtained when other temporal references were used (i.e., SPW trough, ripple onset or CA3 events; Figure S6).

As an alternative way to relate firing patterns to SPW-Rs, we compared the probability of participation of pyramidal cells detected within LFP ripples in either CA1 or CA2 region. CA1 and CA3 pyramidal neurons participated more frequently in CA1 than CA2 ripples during both SLEEP and WAKE (Figure 5D; $p < 0.001$ for all comparisons, signed-rank-sum test). However, the two subpopulations of CA2 cells behaved differently. CA2 phasic cells were more active in CA2 ripples ($p < 0.001$ for all comparison with CA1 and CA3 cells and $p < 0.05$ when compared with CA2 ramping cells, rank-sum test) and they also fired frequently during CA1 ripples ($p < 0.001$ for all comparisons except when compared with CA3c neurons, $p < 0.05$; rank-sum test). In contrast, CA2 ramping cells were rarely recruited during CA1 ripples yet fired robustly during CA2 ripples ($p < 0.001$ for all comparisons, rank-sum test). CA2 cells participated more in CA1 ripples during WAKE than during SLEEP (Figure 5E; $p < 0.01/0.001$ for CA2 phasic/ramping, signed-rank test) but showed no state-dependence in their participation in CA2 ripples ($p > 0.05$). In contrast, CA1 and CA3 cells participated more in both CA1 and CA2 ripples during SLEEP compared to WAKE ($p < 0.001$ for CA1 and $p < 0.01$ for CA3a, b, and c in both types of ripples, signed-rank test). Similar results were obtained when participation in CA3 and CA2 ripple events was compared (Figures S4B and S4C).

In contrast to pyramidal cells, spiking of interneurons in CA1, CA2, and CA3 regions was rather synchronous, peaking approximately 5 ms prior to CA1 SPW-R peak (Figure S5) (Csicsvari et al., 1999, 2000; Stark et al., 2014), in line of previous observations that interneurons show a more global involvement in population events compared to pyramidal cells (Csicsvari et al., 2000). Yet firing rates of CA1 interneurons were lower during WAKE CA1 SPW-Rs than during SLEEP. In contrast, the firing of CA3a interneurons was significantly higher in WAKE than in SLEEP (Figure S5D), which may explain the decreased contribution of CA3a pyramidal cells to WAKE SPW-R initiation.

Overall, these results indicate that the local ensemble activity of neurons in the CA2 region represents the earliest activity in SPW-R events, implicating this region with a potential role in the cascade of events that trigger SPW-Rs.

Inter-regional Neuronal Interactions

In addition to the above population comparisons, we analyzed the inter-regional spike timing between pairs of pyramidal cells in the time windows of CA1 SPW-Rs (Figure 6A). As expected, single CA3 pyramidal neurons, on average, fired earlier than their CA1 partners (6 ms in SLEEP and AWAKE). Spiking of CA2 pyramidal cells preceded both CA1 (SLEEP, 7/10 ms time lag; WAKE, 9/10 ms time lag for CA2 phasic and ramping cells, respectively; Figure 6A) and CA3 pyramidal neurons (SLEEP, 4/8 ms; WAKE, 6/7 ms CA2 phasic/ramping). In addition to the peak delays, the asymmetry of the CA2-CA1 and CA2-CA3 cross-correlograms also supports the leading role of CA2 neurons in SPW-R induction. While CA2 phasic cells typically had cross-correlograms with a sharp peak, CA2 ramping neurons displayed a sustained increase prior to both CA1 and CA3 firing and during both WAKE and SLEEP.

Intra-regional Activation Patterns of Inhibitory Interneurons

Population cross-correlograms between pyramidal neurons and putative interneurons within both CA1 and CA3 regions showed that the peak activation of putative interneurons occurred 2–3 ms earlier than the peak activity of pyramidal cells during both SLEEP and WAKE (Figure 6B), indicating that interneurons are also activated in a feedforward manner from an upstream region (Csicsvari et al., 1999). In contrast, CA2 pyramidal neurons fired before CA2 interneurons (Figure 6B; 3/5 ms for CA2 phasic, 16/13 ms for CA2 ramping in SLEEP and WAKE). Together, these results imply that the earliest participant and the putative initiator of SPW-Rs in the hippocampus is the CA2 pyramidal cell population.

Our large-scale recordings of single neurons also allowed for studying the monosynaptic interactions between regions (Figure 6C; Figure S7A) by calculating spike-transmission probabilities (Berényi et al., 2014; Csicsvari et al., 1998). CA2 pyramidal neurons activated not only local putative interneurons but also interneurons in the CA1 and CA3 regions, although with lower probability in the distal regions than locally (Figure 6D). Among the CA3 subregions, CA3a received more inputs from CA2 than CA3b or CA3c (Figure 6D; $p < 0.01$, unpaired t test). Phasic CA2 neurons were significantly more effective in discharging interneurons in their target CA3 region compared to ramping neurons ($p < 0.05$, t test). CA2 interneurons received not only

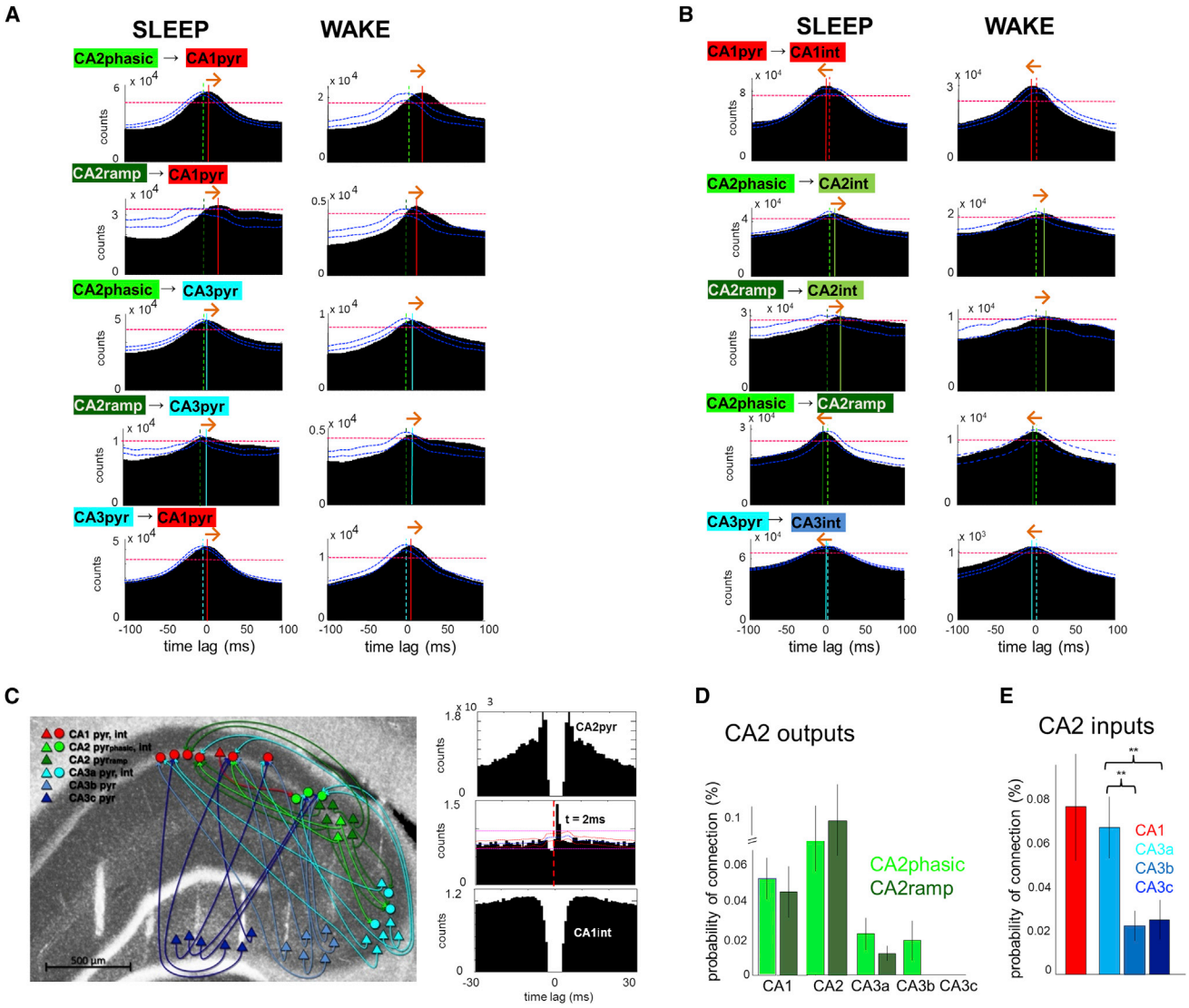

Figure 6. Inter-regional Spike Timing Relationships

(A) Population cross-correlograms of pyramidal cells from different regions were constructed by pooling all spikes that occurred during SPW-R periods during SLEEP and WAKE. Note that CA2 pyramidal cells fired, on average, before CA1 and CA3 principal cells during both SLEEP and WAKE SPW-R, and CA3 units fire earlier than CA1. Dashed vertical lines indicate zero time lag and solid lines mark CCG peaks. Red horizontal dashed lines indicate 0.01% significance level obtained from jittered CCGs and blue curves show the 0.01% significance boundaries for CCG symmetry, obtained by shuffling the order of the individual cell pairs. Orange arrows indicate inferred direction of spike transmission.

(B) Population cross-correlograms between pyramidal cells and interneurons within regions. Note that in CA1 and CA3 the maximal probability of firing of interneurons slightly precedes pyramidal cells (dashed lines), while in CA2 pyramidal cell activation leads interneuron discharge.

(C) Connectivity graph shows putative monosynaptic connections between pyramidal cells (triangles) and interneurons (circles) in a representative session (colors represent region identities). Right panel, cross-correlogram and autocorrelograms of an example CA2 pyramidal cell/CA1 interneuron pair.

(D) CA2 output connectivity was quantified as the probability (±SEM) of monosynaptic connections (significant pairs divided by total possible pairs) between CA2 pyramidal cells and CA1, CA2, or CA3 interneurons.

(E) CA2 input connections were qualified as the probability (±SEM) of connections between CA1 or CA3 pyramidal cells with CA2 interneurons. CA2 interneurons received more inputs from CA3a than from CA3b or c. See also Figure S7.

recurrent excitation from the adjacent CA2 pyramidal cells, but also from CA1 and CA3 pyramidal neurons. The connection probability between CA3a pyramidal cells and CA2 interneurons was significantly higher compared to connections from the CA3b and c subregions (Figure 6E; $p < 0.01$, unpaired t test).

Differential Role of Deep and Superficial CA2 Pyramidal Cells in SPW-Rs

Previous work has shown that deep and superficial substrata of the CA1 pyramidal layer have different physiological features and anatomical connectivity (Mizuseki et al., 2011; Stark et al.,

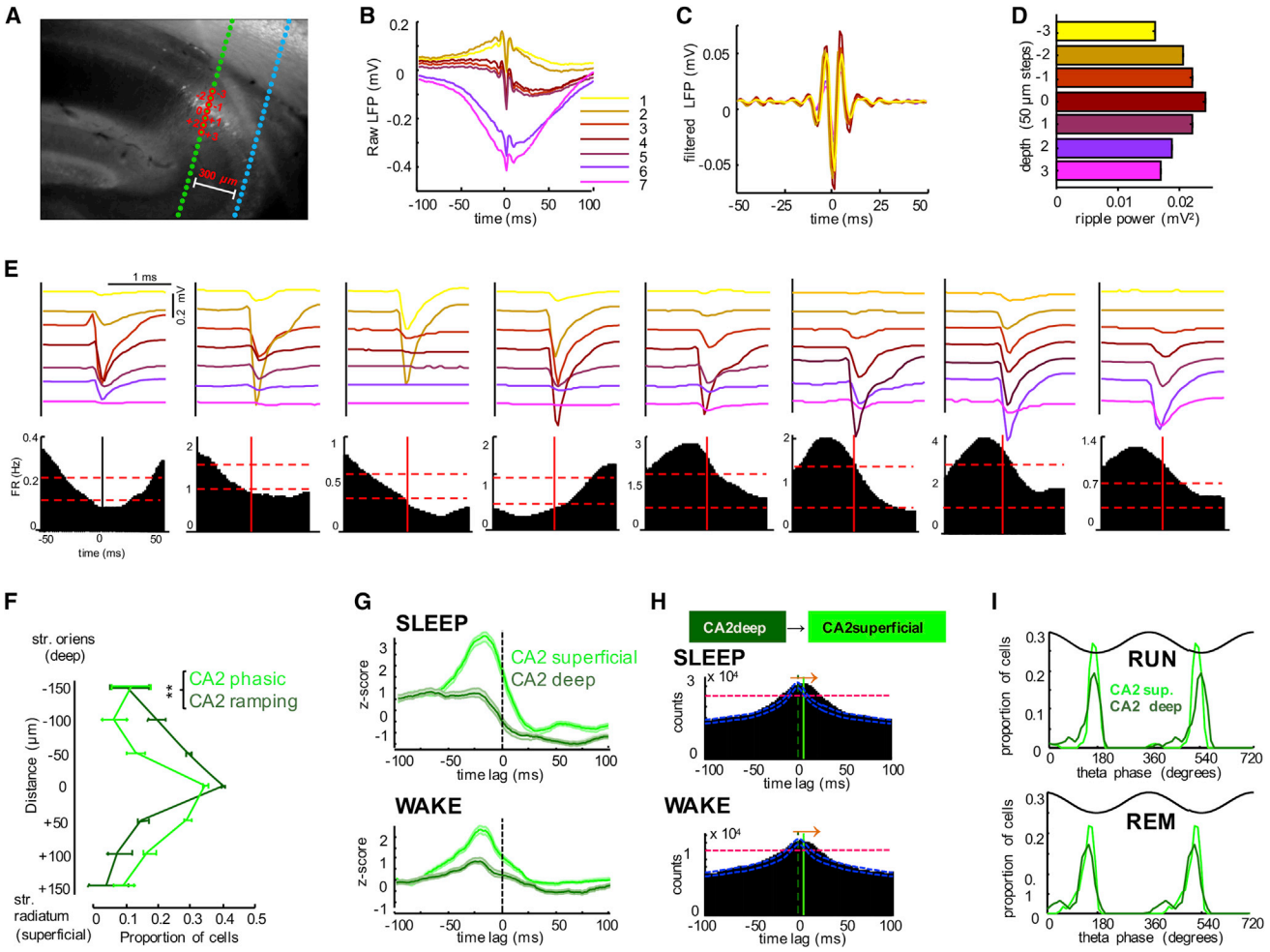

Figure 7. Anatomical Segregation of Phasic and Ramping CA2 Pyramidal Cells

(A) Anti-PCP4 immunolabeled section of the hippocampus with recording shank passing through the CA2 region.

(B) Average LFP traces recorded at different depths in CA2, triggered by CA2 ripple power peaks (n = 2,041).

(C) Filtered (140–230 Hz) traces at different depths.

(D) Mean ripple power at different recording depths.

(E) Average waveforms (top panels) of eight neurons simultaneously recorded by the same shank showing different ripple-related firing patterns (bottom panels). Note that deep neurons are suppressed (1–4), whereas superficial neurons (5–8) are recruited by ripples. Vertical red line at 0 ms, peak of ripple power. Horizontal dashed lines indicate 95% upper and lower confidence intervals.

(F) Depth distribution (±SEM) of phasic and ramping neurons in the CA2 pyramidal layer. Phasic cells were preferably found in superficial pyramidal layer (closer to str. radiatum) while CA2 ramping cells were preferably located in the deep layer (closer to str. oriens).

(G) Peri-SPW-R activity curves were computed as in Figure 5 for superficial and deep CA2 cells, respectively. Note the similarity of activity curves of superficial and deep neurons to phasic and ramping categorization, respectively (compare with Figure 5A).

(H) Peri-SPW-R cross-correlograms between CA2 deep and superficial pyramidal cells during SLEEP and WAKE. Note that deep cells slightly precede the activation of superficial cells.

(I) Distribution of preferred theta phases of unit firings during running and REM sleep periods for CA2 deep and superficial pyramidal cells. See also Figure S7.

2014; Varga et al., 2012). Since in a previous study ripple-suppressed CA1 pyramidal cells were located in deep CA1 pyramidal layer (Valero et al., 2015), we investigated SPW-R-related spiking of neurons as function of their depth location in the CA2 pyramidal layer. The vertical distribution of the recording sites of the silicon probe shanks allowed us to simultaneously sample both superficial and deep neurons. The separation of neurons into "deep" and "superficial" subgroups was facilitated by the larger depth-span of the "electric layer" compared to the narrow anatomical CA1 pyramidal layers (< 100 µm; Stark et al., 2014). The middle of the CA2 pyramidal layer was identified physiologically by the recording site with the largest ripple-amplitude in the local LFP (Mizuseki et al., 2011). We were able to isolate multiple single units at several recording sites in the shank located inside the histologically defined CA2 region (Figure 1A; Figures 7A and 7E). The largest number of units were recorded by electrodes located in the middle of the pyramidal layer (Mizuseki et al., 2011), where both phasic and ramping units

were present (Figure 7E, panels 4 and 5). The physiologically identified phasic and ramping groups showed significantly different depth distributions; ramping neurons resided largely above the middle of the CA2 pyramidal layer (deep, toward str. oriens), and phasic neurons were located mainly below the middle of the layer (superficial; toward str. radiatum) (Figures 7E and 7F; $p < 0.01$, $n = 16$ sessions in five rats, paired t test). CA2 superficial and deep cells had similar overall firing rates, but the deep cells were significantly more bursty, analogous to CA1 sublayer differences (Mizuseki et al., 2011; Figures S7B and S7C). CA1 SPW-R-triggered spike histograms of deep and superficial layer CA2 pyramidal neurons yielded patterns reminiscent of the ramping and phasic subgroups, respectively (Figure 7G). Activation of deep sublayer neurons preceded the discharge of superficial neurons during SPW-R (Figure 7H), resembling the pattern observed for CA2 ramping and phasic cells (Figure 6B).

Because CA1, but not CA3, neurons show characteristic sublayer-dependent phase coupling to theta oscillations during waking and REM sleep (Mizuseki et al., 2011), we also quantified these parameters for superficial and deep sublayer CA2 neurons. All CA2 pyramidal neurons in both sublayers kept their theta phase preference across waking and REM sleep (Figure 7I; Figure S7E), indicating that in this respect they are more similar to CA3 than CA1 pyramidal cells. Although our recordings cannot fully exclude a limited contamination from the adjacent CA3a pyramidal cells in every case, the findings clearly show that the superficial and deep layer CA2 pyramidal neurons behave differently. Furthermore, superficial CA2 neurons may share many features with their adjacent CA3a partners.

DISCUSSION

Our findings show that increased discharge of CA2 pyramidal cells precedes the activation of their CA3 peers during SPW-Rs. Deep layer CA2 neurons ramp up their activity first, followed by suppression of their spiking during SPW-Rs. Superficial CA2 neurons fire, as a population, prior to synchronized activity of CA3 neurons. The population activation spreads through CA3a-b and c and finally to CA1 stratum radiatum where it elicits an LFP SPW (current sink). Although CA2 neurons contribute to SPW-Rs during both sleeping and waking, their contribution to wake events is stronger (Figure 5). A subset of CA2 ripples are followed by a sink in CA1 stratum oriens, indicating direct induction of CA1 ripples by the CA2 input. Overall, these results establish a prominent role of the CA2 region in SPW-R generation.

Mechanisms of SPW-R Initiation

Self-organized SPW-Rs have been postulated to arise in the CA3 region when decreased activity of subcortical neuromodulators allows the spread of excitation in its strongly recurrent network (Buzsáki et al., 1983; Csicsvari et al., 2000; Mann and Paulsen, 2007; Schlingloff et al., 2014; Ylinen et al., 1995). Most CA3 recurrent collaterals arise from the CA3a subregion, and these neurons contribute relatively little to direct excitation of CA1 neurons. The ratio of recurrent versus CA1-projecting axon collaterals increases gradually from CA3a to CA3b and CA3c subregions (Ishizuka et al., 1990; Li et al., 1994). In addition to CA3a, CA2 neurons also contribute strongly to the CA2-CA3 recurrent system and send a minority of their axons to the basal dendrites of CA1 pyramidal cells (Li et al., 1994; Tamamaki et al., 1988). The physiological spread of activity appears to obey this anatomical organization (Csicsvari et al., 2000, 2003). In our experiments, the earliest excitability change was detected in the deep layer ramping neurons, whose activity gradually increased tens of milliseconds prior to the SPW-R without culminating in their synchronous population burst (Figure 5). Such ramping up of excitatory activity is also observable in the membrane potential of CA3 neurons as increasing amplitude of EPSCs 50–100 ms before the SPW-R event (Schlingloff et al., 2014) and is considered to be critical for giving rise to large population events (Traub and Wong, 1982). Thus, ramping up their activity, deep CA2 pyramidal neurons play a leading role in the initiation of populations bursts.

Ramping CA2 neurons became suppressed at the onset of SPW population burst of phasic CA2 neurons and the recruitment of CA3 and CA1 populations. The hypothesized population burst-triggering ability of the CA2 circuit might be explained by its unique anatomical wiring (Figure 1B). In addition to local feedback excitation, CA2 interneurons were also activated by CA1 and CA3 pyramidal neurons, in agreement with anatomical and physiological findings (Bartesaghi et al., 2006; Chevaleyre and Siegelbaum, 2010; Mercer et al., 2012; Piskorowski and Chevaleyre, 2012, 2013). Phasic (superficial) CA2 pyramidal cells were more effective in driving local interneurons compared to their ramping (deep) peers (Figure 6D), a feature that they share with the CA1 region (Lee et al., 2014; Stark et al., 2014; Valero et al., 2015). Thus, the strong excitation of CA2 interneurons by phasic CA2, CA3, and CA1 pyramidal neurons participating in SPW-R population bursts may explain the strong silencing of the event-initiator ramping neurons (Kay et al., 2016). Such feedback mechanisms may effectively prevent excessive recruitment of pyramidal neurons during the emerging network bursts underlying SPW-Rs and their excessive repetitive occurrences. In support of this hypothesis, when fast $GABA_A$ inhibition is suppressed pharmacologically by picrotoxin, large amplitude interictal spikes can be triggered by weak electrical stimulation. Importantly, interictal events invariably emerge in the CA2 region, independent of the site of stimulation from where the population bursts spread to CA3b and c and eventually invade the CA1 region (Traub and Wong, 1982). The high excitability state of the CA2 region is also supported by in vivo models of epilepsy in rodents and human patients, which show that pathological "fast-ripples" (> 250 Hz) occur more frequently in the CA2 compared to CA1 and CA3 regions (Bragin et al., 1999a, 1999b; Ibarz et al., 2010).

Relationship to Epileptic Interictal Events

In addition to "regular" SPW-R events with a negative SPW in CA1 str. radiatum, in a minority of cases we observed that CA2 activity was followed by a short latency (~5 ms) negative wave in CA1 str. oriens and a positive SPW in str. radiatum, accompanied by a ripple in the pyramidal layer (Figure 1C). The likely anatomical substrate of this pattern is the associational collaterals of CA2 and CA3a neurons that innervate the basal dendrites of CA1 pyramidal cells (Ishizuka et al., 1990; Li et al., 1994). Activation of this pathway, therefore, can induce an active

sink in str. oriens and an associated passive return current (source) in str. radiatum and lacunosum-moleculare. Most often, however, the initial str. oriens negativity was followed by a later negative SPW in str. radiatum and a concurrent ripple, an indication that the direct CA2-CA1 excitation was coupled with multisynaptic recruitment of CA1 neurons via the CA2—CA3a—CA3b—CA3c route. These experiments, therefore, show that strong activation of CA1 pyramidal cells and partner interneurons are sufficient to induce a ripple, irrespective of the source of excitation (Nakashiba et al., 2009; Stark et al., 2014). They also demonstrate that short-latency "priming" of the CA1 circuit by the direct CA2 and CA3a inputs can be combined with a longer-latency, more complex recruitment of other CA3 neurons. These observations also shed light on a long-held paradox of the origin of two types of interictal spikes in various models of epilepsy (Alvarado-Rojas et al., 2015; Wadman et al., 1983). Type I interictal spikes are "exaggerated" versions of physiological SPWs. Accordingly, Type I LFP spikes are negative in CA1 str. radiatum, and they utilize the same anatomical substrates as SPWs, but they are considerable larger in amplitude and shorter in duration, often combined with one or more large amplitude population spikes in the CA1 pyramidal layer (Buzsáki et al., 1991). In contrast, Type II interictal spikes have positive polarity in CA1 str. radiatum, and their mechanism is unknown (Wadman et al., 1983). In light of our present observations, Type II interictal spikes may be supported by super-strong excitation of the basal dendrites of CA1 pyramidal neurons by the direct CA2—CA1 path. Similar LFP patterns, i.e., positive and negative polarity SPW in the stratum radiatum accompanying CA1 ripples, were also observed in monkeys and were associated with different patterns of brain-wide BOLD activation (Ramirez-Villegas et al., 2015). This suggest the possibility that CA2- and CA3-initiated SPW-R events reach different target regions or are under the control of distinct subcortical inputs.

SPW-Rs in the Waking and Sleeping Brain

A striking observation of the present experiments was the characteristically different involvement of the CA2 region in ripples during waking and sleep. This is perhaps not surprising since in the sleeping animal activity of subcortical neuromodulators is considerably more strongly attenuated than in the waking but still animal (Csicsvari et al., 2007; Karlsson and Frank, 2009; O'Neill et al., 2006). The frequency of CA1 ripples is faster during waking immobility than during non-REM sleep (Buzsáki, 2015; Ponomarenko et al., 2008), and this difference is also present in CA2. We also found that while both baseline firing rates and CA1 SPW-R-related spiking of CA1 and CA3 pyramidal neurons decreased during waking compared to non-REM, CA2 neurons were more active during waking. The relative incidence of SPW-Rs in CA1 was higher during non-REM compared to waking, whereas the incidence of CA2-confined ripples was higher during waking. Sleep CA1 SPW-Rs frequently co-occurred with CA3 ripples, but such local CA3 ripples were rare during waking. In contrast, wake SPW-Rs were commonly preceded by large amplitude and faster frequency CA2 LFP ripples (Figure 3D). Such brain state-region interactions could, in principle, be brought about by the differential control of the supramammillary projection, which selectively innervates the CA2 region (Maglóczky et al., 1994). These physiological differences can impact the role played by SPW-Rs in the waking and sleeping brain. Reduction or blockade of SPW-Rs during post-learning sleep can interfere with memory consolidation (Ego-Stengel and Wilson, 2010; Girardeau et al., 2009). Elimination of SPW-Rs in the waking rat, on the other hand, interferes with working memory and prospective route-planning (Girardeau et al., 2009; Jadhav et al., 2012). One possible mechanism for this difference is the selective access of the entorhinal cortex to the CA2 region (Chevaleyre and Siegelbaum, 2010), whose efficacy may change with brain state. Our findings suggest that during waking, the entorhinal cortex may "prime" the CA2 region so that prospective (forward) replay may dominate SPW-R content, whereas during sleep the CA3 region plays a more important role in triggering SPW events and induces replay of reverse neuronal sequences.

Given the critical role of SPW-Rs in memory consolidation, the finding that CA2 disruption did not affect spatial memory performance (Hitti and Siegelbaum, 2014) is seemingly at odds with our findings that the CA2 region initiates SPW-Rs. However, ripples can emerge at multiple hippocampal subregions, provided that sufficient level of excitation is built up locally (Stark et al., 2014). In the absence of CA2, the neighboring CA3a subregion can likely become the SPW-R-initiator zone, given its similarly extensive local excitatory collateral system (Tamamaki et al., 1988).

The phasic and ramping CA2 pyramidal cells likely correspond to the two subgroups of neurons ("positively" and "negatively" modulated by ripples) described by Kay et al. (2016). However, Kay et al. (2016) concluded that CA2 neurons are strongly suppressed during SPW-Rs (i.e., our ramping neurons) and suggested that positively modulated (our phasic group) neurons are in fact CA2-bordering CA3a or CA1 pyramidal cells. Our high-spatial-resolution recording methods, the large coverage of the CA1-2-3 regions, and the histologically identified recording sites within the CA2 region unequivocally demonstrate that the CA2 region consists of sublayers with physiologically and, possibly, anatomically distinct properties. Overall, our findings demonstrate that the strongly recurrent CA2 region is a high excitability zone, which can function as the initiator of population events.

EXPERIMENTAL PROCEDURES

Eight rats were implanted with 256-sites movable silicon probes (Berényi et al., 2014; Schomburg et al., 2014; see Supplemental Experimental Procedures for full details). Animals were recorded during long SLEEP sessions in their home cage (1–5 hr) and during different navigational tasks (open field exploration, linear track running). All experiments were performed in accordance with European Union guidelines (2003/65/CE) and the National Institutes of Health Guidelines for the Care and Use of Animals for Experimental Procedures. The experimental protocols were approved by the Ethical Committee for Animal Research at the Albert Szent-Györgyi Medical and Pharmaceutical Center of the University of Szeged and the Animal Care and Use Committee of the New York University Medical Center.

Cellular and dendritic layers were identified by CSD and ICA analysis of LFPs (Fernández-Ruiz et al., 2013; Schomburg et al., 2014). The CA2 region was identified post hoc from histological sections by the thicker pyramidal layer and wider and sparser cell bodies compared to CA1 and confirmed by specific immunolabeling (Figure 1A; anti-PCP4).

Data analyses were carried out using built-in and custom-built software in Matlab (MathWorks). Significance testing of data comparisons was done by

standard parametric (Student's t test) and non-parametric (Wilcoxon signed-rank or rank-sum tests) tests or by determining the crossings of confidence boundaries of surrogate datasets (compensated for type I statistical error). Single, double, and triple asterisks on the figures represent significance levels lower than 0.05, 0.01, and 0.001, respectively. For all plots, mean and standard error are shown, unless otherwise noted.

SUPPLEMENTAL INFORMATION

Supplemental Information includes Supplemental Experimental Procedures, seven figures, and one table and can be found with this article online at http://dx.doi.org/10.1016/j.neuron.2016.08.008.

AUTHOR CONTRIBUTIONS

The experiments were conceived and designed by all authors. Recordings were performed by A.O., A.F.-R., and A.B. A.O. and A.F.-R. analyzed the data and performed immunohistological characterizations. The paper was written by G.B., A.O., A.F.-R., and A.B.

ACKNOWLEDGMENTS

We thank Brendon Watson, Daniel English, Eran Stark, Viktor Varga, Norbert Hájos, and Yuichi Takeuchi for insightful comments; Péter Hegyi for providing access to confocal microscopy; Gergő Nagy for experimental assistance; Liset Menendez de la Prida and Elena Cid for providing immunohistological procedures and discussions; Miguel Sancho, Sagrario Muñoz, and Ricardo Bajo for constant support and advice. This work was supported by EU-FP7-ERC-2013-Starting grant (No. 337075), the "Momentum" Program of the Hungarian Academy of Sciences (LP2013-62/2013), NIHMH54671, MH107396, the Simons Foundation, NS 090583, Fundación La Caixa, and EMBO (ALTF 147-2015). A.B. is the founder and owner of Amplipex Ltd., Szeged, Hungary, which manufactures signal-multiplexed head stages and demultiplexing systems. The other authors have nothing to disclose.

Received: February 26, 2016
Revised: May 17, 2016
Accepted: July 29, 2016
Published: September 1, 2016

REFERENCES

Alexander, G.M., Farris, S., Pirone, J.R., Zheng, C., Colgin, L.L., and Dudek, S.M. (2016). Social and novel contexts modify hippocampal CA2 representations of space. Nat. Commun. *7*, 10300.

Alvarado-Rojas, C., Huberfeld, G., Baulac, M., Clemenceau, S., Charpier, S., Miles, R., de la Prida, L.M., and Le Van Quyen, M. (2015). Different mechanisms of ripple-like oscillations in the human epileptic subiculum. Ann. Neurol. *77*, 281–290.

Amaral, D., and Lavenex, P. (2006). Hippocampal Neuroanatomy. In The Hippocampus Book, P. Andersen, R. Morris, D. Amaral, T. Bliss, and J. O'Keefe, eds. (Oxford University Press), pp. 37–114.

Babb, T.L., Lieb, J.P., Brown, W.J., Pretorius, J., and Crandall, P.H. (1984). Distribution of pyramidal cell density and hyperexcitability in the epileptic human hippocampal formation. Epilepsia *25*, 721–728.

Bartesaghi, R., Migliore, M., and Gessi, T. (2006). Input-output relations in the entorhinal cortex-dentate-hippocampal system: evidence for a non-linear transfer of signals. Neuroscience *142*, 247–265.

Benes, F.M., and Berretta, S. (2001). GABAergic interneurons: implications for understanding schizophrenia and bipolar disorder. Neuropsychopharmacology *25*, 1–27.

Benes, F.M., Kwok, E.W., Vincent, S.L., and Todtenkopf, M.S. (1998). A reduction of nonpyramidal cells in sector CA2 of schizophrenics and manic depressives. Biol. Psychiatry *44*, 88–97.

Berényi, A., Somogyvári, Z., Nagy, A.J., Roux, L., Long, J.D., Fujisawa, S., Stark, E., Leonardo, A., Harris, T.D., and Buzsáki, G. (2014). Large-scale, high-density (up to 512 channels) recording of local circuits in behaving animals. J. Neurophysiol. *111*, 1132–1149.

Braak, E., Braak, H., Strenge, H., and Muhtaroglu, A.U. (1980). Age-related alterations of the proximal axon segment in lamina IIIab-pyramidal cells of the human isocortex. A Golgi and fine structural study. J. Hirnforsch. *21*, 531–535.

Bragin, A., Engel, J., Jr., Wilson, C.L., Fried, I., and Buzsáki, G. (1999a). High-frequency oscillations in human brain. Hippocampus *9*, 137–142.

Bragin, A., Engel, J., Jr., Wilson, C.L., Fried, I., and Mathern, G.W. (1999b). Hippocampal and entorhinal cortex high-frequency oscillations (100–500 Hz) in human epileptic brain and in kainic acid–treated rats with chronic seizures. Epilepsia *40*, 127–137.

Buzsáki, G. (2015). Hippocampal sharp wave-ripple: A cognitive biomarker for episodic memory and planning. Hippocampus *25*, 1073–1188.

Buzsáki, G., Leung, L.W., and Vanderwolf, C.H. (1983). Cellular bases of hippocampal EEG in the behaving rat. Brain Res. *287*, 139–171.

Buzsáki, G., Hsu, M., Slamka, C., Gage, F.H., and Horváth, Z. (1991). Emergence and propagation of interictal spikes in the subcortically denervated hippocampus. Hippocampus *1*, 163–180.

Buzsáki, G., Horváth, Z., Urioste, R., Hetke, J., and Wise, K. (1992). High-frequency network oscillation in the hippocampus. Science *256*, 1025–1027.

Chevaleyre, V., and Siegelbaum, S.A. (2010). Strong CA2 pyramidal neuron synapses define a powerful disynaptic cortico-hippocampal loop. Neuron *66*, 560–572.

Csicsvari, J., Hirase, H., Czurko, A., and Buzsáki, G. (1998). Reliability and state dependence of pyramidal cell-interneuron synapses in the hippocampus: an ensemble approach in the behaving rat. Neuron *21*, 179–189.

Csicsvari, J., Hirase, H., Czurkó, A., Mamiya, A., and Buzsáki, G. (1999). Fast network oscillations in the hippocampal CA1 region of the behaving rat. J. Neurosci. *19*, RC20.

Csicsvari, J., Hirase, H., Mamiya, A., and Buzsáki, G. (2000). Ensemble patterns of hippocampal CA3-CA1 neurons during sharp wave-associated population events. Neuron *28*, 585–594.

Csicsvari, J., Jamieson, B., Wise, K.D., and Buzsáki, G. (2003). Mechanisms of gamma oscillations in the hippocampus of the behaving rat. Neuron *37*, 311–322.

Csicsvari, J., O'Neill, J., Allen, K., and Senior, T. (2007). Place-selective firing contributes to the reverse-order reactivation of CA1 pyramidal cells during sharp waves in open-field exploration. Eur. J. Neurosci. *26*, 704–716.

Cui, Z., Gerfen, C.R., and Young, W.S., 3rd (2013). Hypothalamic and other connections with dorsal CA2 area of the mouse hippocampus. J. Comp. Neurol. *521*, 1844–1866.

Dam, A.M. (1980). Epilepsy and neuron loss in the hippocampus. Epilepsia *21*, 617–629.

Ding, S.L., Haber, S.N., and Van Hoesen, G.W. (2010). Stratum radiatum of CA2 is an additional target of the perforant path in humans and monkeys. Neuroreport *21*, 245–249.

Dudek, S.M., Alexander, G.M., and Farris, S. (2016). Rediscovering area CA2: unique properties and functions. Nat. Rev. Neurosci. *17*, 89–102.

Ego-Stengel, V., and Wilson, M.A. (2010). Disruption of ripple-associated hippocampal activity during rest impairs spatial learning in the rat. Hippocampus *20*, 1–10.

English, D.F., Peyrache, A., Stark, E., Roux, L., Vallentin, D., Long, M.A., and Buzsáki, G. (2014). Excitation and inhibition compete to control spiking during hippocampal ripples: intracellular study in behaving mice. J. Neurosci. *34*, 16509–16517.

Fernández-Ruiz, A., Makarov, V.A., Benito, N., and Herreras, O. (2012). Schaffer-specific local field potentials reflect discrete excitatory events at gamma frequency that may fire postsynaptic hippocampal CA1 units. J. Neurosci. *32*, 5165–5176.

Fernández-Ruiz, A., Muñoz, S., Sancho, M., Makarova, J., Makarov, V.A., and Herreras, O. (2013). Cytoarchitectonic and dynamic origins of giant positive local field potentials in the dentate gyrus. J. Neurosci. *33*, 15518–15532.

Girardeau, G., Benchenane, K., Wiener, S.I., Buzsáki, G., and Zugaro, M.B. (2009). Selective suppression of hippocampal ripples impairs spatial memory. Nat. Neurosci. *12*, 1222–1223.

Gloor, P. (1991). Preoperative electroencephalographic investigation in temporal lobe epilepsy: extracranial and intracranial recordings. Can. J. Neurol. Sci. *18* (4, Suppl), 554–558.

Hitti, F.L., and Siegelbaum, S.A. (2014). The hippocampal CA2 region is essential for social memory. Nature *508*, 88–92.

Ibarz, J.M., Foffani, G., Cid, E., Inostroza, M., and Menendez de la Prida, L. (2010). Emergent dynamics of fast ripples in the epileptic hippocampus. J. Neuroscience *30*, 16249–16261.

Ishizuka, N., Weber, J., and Amaral, D.G. (1990). Organization of intrahippocampal projections originating from CA3 pyramidal cells in the rat. J. Comp. Neurol. *295*, 580–623.

Ishizuka, N., Cowan, W.M., and Amaral, D.G. (1995). A quantitative analysis of the dendritic organization of pyramidal cells in the rat hippocampus. J. Comp. Neurol. *362*, 17–45.

Jadhav, S.P., Kemere, C., German, P.W., and Frank, L.M. (2012). Awake hippocampal sharp-wave ripples support spatial memory. Science *336*, 1454–1458.

Karlsson, M.P., and Frank, L.M. (2009). Awake replay of remote experiences in the hippocampus. Nat. Neurosci. *12*, 913–918.

Kay, K., Sosa, M., Chung, J.E., Karlsson, M.P., Larkin, M.C., and Frank, L.M. (2016). A hippocampal network for spatial coding during immobility and sleep. Nature *531*, 185–190.

Kirino, T. (1982). Delayed neuronal death in the gerbil hippocampus following ischemia. Brain Res. *239*, 57–69.

Knable, M.B., Barci, B.M., Webster, M.J., Meador-Woodruff, J., and Torrey, E.F.; Stanley Neuropathology Consortium (2004). Molecular abnormalities of the hippocampus in severe psychiatric illness: postmortem findings from the Stanley Neuropathology Consortium. Mol. Psychiatry *9*, 609–620.

Kohara, K., Pignatelli, M., Rivest, A.J., Jung, H.Y., Kitamura, T., Suh, J., Frank, D., Kajikawa, K., Mise, N., Obata, Y., et al. (2014). Cell type-specific genetic and optogenetic tools reveal hippocampal CA2 circuits. Nat. Neurosci. *17*, 269–279.

Kotloski, R., Lynch, M., Lauersdorf, S., and Sutula, T. (2002). Repeated brief seizures induce progressive hippocampal neuron loss and memory deficits. Prog. Brain Res. *135*, 95–110.

Lee, S.H., Marchionni, I., Bezaire, M., Varga, C., Danielson, N., Lovett-Barron, M., Losonczy, A., and Soltesz, I. (2014). Parvalbumin-positive basket cells differentiate among hippocampal pyramidal cells. Neuron *82*, 1129–1144.

Lein, E.S., Zhao, X., and Gage, F.H. (2004). Defining a molecular atlas of the hippocampus using DNA microarrays and high-throughput in situ hybridization. J. Neurosci. *24*, 3879–3889.

Li, X.G., Somogyi, P., Ylinen, A., and Buzsáki, G. (1994). The hippocampal CA3 network: an in vivo intracellular labeling study. J. Comp. Neurol. *339*, 181–208.

Lorente de Nó, R. (1947). A study of nerve physiology. In Studies from the Rockefeller Institute for Medical Research, *Vol. 131*Studies from the Rockefeller Institute for Medical Research (Rockefeller Institute for Medical Research), pp. 1–496.

Maglóczky, Z., Acsády, L., and Freund, T.F. (1994). Principal cells are the postsynaptic targets of supramammillary afferents in the hippocampus of the rat. Hippocampus *4*, 322–334.

Mankin, E.A., Diehl, G.W., Sparks, F.T., Leutgeb, S., and Leutgeb, J.K. (2015). Hippocampal CA2 activity patterns change over time to a larger extent than between spatial contexts. Neuron *85*, 190–201.

Mann, E.O., and Paulsen, O. (2007). Role of GABAergic inhibition in hippocampal network oscillations. Trends Neurosci. *30*, 343–349.

Mercer, A., Eastlake, K., Trigg, H.L., and Thomson, A.M. (2012). Local circuitry involving parvalbumin-positive basket cells in the CA2 region of the hippocampus. Hippocampus *22*, 43–56.

Mizuseki, K., Diba, K., Pastalkova, E., and Buzsáki, G. (2011). Hippocampal CA1 pyramidal cells form functionally distinct sublayers. Nat. Neurosci. *14*, 1174–1181.

Nadler, J.V., Perry, B.W., and Cotman, C.W. (1978). Intraventricular kainic acid preferentially destroys hippocampal pyramidal cells. Nature *271*, 676–677.

Nakashiba, T., Buhl, D.L., McHugh, T.J., and Tonegawa, S. (2009). Hippocampal CA3 output is crucial for ripple-associated reactivation and consolidation of memory. Neuron *62*, 781–787.

Narr, K.L., Bilder, R.M., Kim, S., Thompson, P.M., Szeszko, P., Robinson, D., Luders, E., and Toga, A.W. (2004). Abnormal gyral complexity in first-episode schizophrenia. Biol. Psychiatry *55*, 859–867.

Nullmeier, S., Panther, P., Dobrowolny, H., Frotscher, M., Zhao, S., Schwegler, H., and Wolf, R. (2011). Region-specific alteration of GABAergic markers in the brain of heterozygous reeler mice. Eur. J. Neurosci. *33*, 689–698.

O'Neill, J., Senior, T., and Csicsvari, J. (2006). Place-selective firing of CA1 pyramidal cells during sharp wave/ripple network patterns in exploratory behavior. Neuron *49*, 143–155.

Patel, J., Fujisawa, S., Berényi, A., Royer, S., and Buzsáki, G. (2012). Traveling theta waves along the entire septotemporal axis of the hippocampus. Neuron *75*, 410–417.

Piskorowski, R.A., and Chevaleyre, V. (2012). Synaptic integration by different dendritic compartments of hippocampal CA1 and CA2 pyramidal neurons. Cell. Mol. Life Sci. *69*, 75–88.

Piskorowski, R.A., and Chevaleyre, V. (2013). Delta-opioid receptors mediate unique plasticity onto parvalbumin-expressing interneurons in area CA2 of the hippocampus. J. Neurosci. *33*, 14567–14578.

Piskorowski, R.A., Nasrallah, K., Diamantopoulou, A., Mukai, J., Hassan, S.I., Siegelbaum, S.A., Gogos, J.A., and Chevaleyre, V. (2016). Age-Dependent Specific Changes in Area CA2 of the Hippocampus and Social Memory Deficit in a Mouse Model of the 22q11.2 Deletion Syndrome. Neuron *89*, 163–176.

Ponomarenko, A.A., Li, J.S., Korotkova, T.M., Huston, J.P., and Haas, H.L. (2008). Frequency of network synchronization in the hippocampus marks learning. Eur. J. Neurosci. *27*, 3035–3042.

Ramirez-Villegas, J.F., Logothetis, N.K., and Besserve, M. (2015). Diversity of sharp-wave-ripple LFP signatures reveals differentiated brain-wide dynamical events. Proc. Natl. Acad. Sci. USA *112*, E6379–E6387.

Rowland, D.C., and Moser, M.B. (2013). Time finds its place in the hippocampus. Neuron *78*, 953–954.

Sadowski, M., Wisniewski, H.M., Jakubowska-Sadowska, K., Tarnawski, M., Lazarewicz, J.W., and Mossakowski, M.J. (1999). Pattern of neuronal loss in the rat hippocampus following experimental cardiac arrest-induced ischemia. J. Neurol. Sci. *168*, 13–20.

Schlingloff, D., Káli, S., Freund, T.F., Hájos, N., and Gulyás, A.I. (2014). Mechanisms of sharp wave initiation and ripple generation. J. Neurosci. *34*, 11385–11398.

Schomburg, E.W., Fernández-Ruiz, A., Mizuseki, K., Berényi, A., Anastassiou, C.A., Koch, C., and Buzsáki, G. (2014). Theta phase segregation of input-specific gamma patterns in entorhinal-hippocampal networks. Neuron *84*, 470–485.

Sloviter, R.S. (1989). Calcium-binding protein (calbindin-D28k) and parvalbumin immunocytochemistry: localization in the rat hippocampus with specific reference to the selective vulnerability of hippocampal neurons to seizure activity. J. Comp. Neurol. *280*, 183–196.

Smith, A.S., Williams Avram, S.K., Cymerblit-Sabba, A., Song, J., and Young, W.S. (2016). Targeted activation of the hippocampal CA2 area strongly enhances social memory. Mol. Psychiatry *21*, 1137–1144.

Stark, E., Roux, L., Eichler, R., Senzai, Y., Royer, S., and Buzsáki, G. (2014). Pyramidal cell-interneuron interactions underlie hippocampal ripple oscillations. Neuron *83*, 467–480.

Sullivan, D., Csicsvari, J., Mizuseki, K., Montgomery, S., Diba, K., and Buzsáki, G. (2011). Relationships between hippocampal sharp waves, ripples, and fast gamma oscillation: influence of dentate and entorhinal cortical activity. J. Neurosci. *31*, 8605–8616.

Tamamaki, N., Abe, K., and Nojyo, Y. (1988). Three-dimensional analysis of the whole axonal arbors originating from single CA2 pyramidal neurons in the rat hippocampus with the aid of a computer graphic technique. Brain Res. *452*, 255–272.

Traub, R.D., and Wong, R.K. (1982). Cellular mechanism of neuronal synchronization in epilepsy. Science *216*, 745–747.

Valero, M., Cid, E., Averkin, R.G., Aguilar, J., Sanchez-Aguilera, A., Viney, T.J., Gomez-Dominguez, D., Bellistri, E., and de la Prida, L.M. (2015). Determinants of different deep and superficial CA1 pyramidal cell dynamics during sharp-wave ripples. Nat. Neurosci. *18*, 1281–1290.

Varga, C., Golshani, P., and Soltesz, I. (2012). Frequency-invariant temporal ordering of interneuronal discharges during hippocampal oscillations in awake mice. Proc. Natl. Acad. Sci. USA *109*, E2726–E2734.

Wadman, W.J., Da Silva, F.H., and Leung, L.W. (1983). Two types of interictal transients of reversed polarity in rat hippocampus during kindling. Electroencephalogr. Clin. Neurophysiol. *55*, 314–319.

Wintzer, M.E., Boehringer, R., Polygalov, D., and McHugh, T.J. (2014). The hippocampal CA2 ensemble is sensitive to contextual change. J. Neurosci. *34*, 3056–3066.

Woodhams, P.L., Celio, M.R., Ulfig, N., and Witter, M.P. (1993). Morphological and functional correlates of borders in the entorhinal cortex and hippocampus. Hippocampus *3*, 303–311.

Ylinen, A., Bragin, A., Nádasdy, Z., Jandó, G., Szabó, I., Sik, A., and Buzsáki, G. (1995). Sharp wave-associated high-frequency oscillation (200 Hz) in the intact hippocampus: network and intracellular mechanisms. J. Neurosci. *15*, 30–46.

Young, W.S., Li, J., Wersinger, S.R., and Palkovits, M. (2006). The vasopressin 1b receptor is prominent in the hippocampal area CA2 where it is unaffected by restraint stress or adrenalectomy. Neuroscience *143*, 1031–1039.

Zhang, Z.J., and Reynolds, G.P. (2002). A selective decrease in the relative density of parvalbumin-immunoreactive neurons in the hippocampus in schizophrenia. Schizophr. Res. *55*, 1–10.